Effects of mechanical nonlinearity of viscoelastic dampers on the seismic performance of viscoelasticlly damped structures

Citation for published version:
Li, Q, Xu, Z, Dong, Y, He, Z, Zhu, C & Lu, Y 2021, 'Effects of mechanical nonlinearity of viscoelastic dampers on the seismic performance of viscoelasticlly damped structures', *Soil Dynamics and Earthquake Engineering*, vol. 150, 106936. https://doi.org/10.1016/j.soildyn.2021.106936

Digital Object Identifier (DOI):
10.1016/j.soildyn.2021.106936

Link:
Link to publication record in Edinburgh Research Explorer

Document Version:
Peer reviewed version

Published In:
Soil Dynamics and Earthquake Engineering

Effects of Mechanical Nonlinearity of Viscoelastic Dampers on the Seismic Performance of Viscoelasticlly Damped Structures

Qiang-Qiang Li[1], Zhao-Dong Xu[1*], Yao-Rong Dong[1], Zhen-Hua He[2], Chen Zhu[1], Yong Lu[1,3]

[1] *Key Laboratory of C&PC Structures of the Ministry of Education, Southeast University, Nanjing, China*

[2] *School of Civil Engineering, Xi'an University of Architecture and Technology, Xi'an, China*

[3] *Institute for Infrastructure and Environment, School of Engineering, The University of Edinburgh, UK*

Correspondence author: zhdxu@163.com

Abstract: Viscoelastic (VE) damper exhibits significant mechanical nonlinearity under dynamic loads due to variations in the temperature, excitation frequency, and the occurrence of large strains. However, in the existing research literature, such nonlinearity is barely considered, and its effects on the aseismic behaviours of viscoelasticlly damped structure (referred to as VE structures) are also unclear. In this paper, a modified equivalent fractional Kelvin model is established to depict the mechanical nonlinearity of VE damper with the introduction of internal variable parameters. Through the comparison with the existing mathematical models for the performance of an individual VE damper, it is found that the proposed model has a high prediction accuracy, especially in the large-strain working condition. To incorporate the effects of real-time change of the mechanical properties of VE dampers on the seismic responses of structures equipped with such dampers, an approximate method is devised for the numerical calculations. Two representative VE structure with proportionally and non-proportionally damped system are analysed with consideration of the time-varying mechanical nonlinearity of VE dampers. The discrepancy between the seismic responses of the VE structure with and without considering the nonlinearity is discussed. The results indicate that the mechanical nonlinearity of VE dampers could introduce a negative effect on the actual seismic resistance capacity of a VE structure, leading potentially to the structure not meeting the design requirements of codes

when the mechanical nonlinearity occurs. The study concludes that it is necessary to take the mechanical nonlinearity into account in the design and performance evaluation of VE structures.

Keywords: VE damper; Mechanical nonlinearity; Mathematic model of VE damper; Seismic analysis; VE structure

1 Introduction

In early applications, VE damper was more often applied in the wind vibration control of the high-rise structures and showed remarkable control effects [1]. With the frequent occurrence of strong earthquakes causing enormous damage, studies on the application of VE dampers for structure were carried out in the seismic regions in the last few decades [2, 3].

Under different work environments, such as different ambient temperature or excitation frequency, changes may occur in the complex network-chain structure, leading to a strong nonlinearity in the mechanical behaviour of VE material. Studies by many researchers have revealed the variation of mechanical properties of VE dampers with temperature and frequency [4, 5]. Besides, when deformed, the molecular chain structure formed between internal molecular chains will be stretched, compressed, or even destroyed, thus exhibiting different configurations, and make the performance of VE material show a strong strain dependency [6, 7].

Although the development of VE damper in building structures has advanced, the normal working strain range is often limited in practice. It has been suggested in [2] that the maximum strain of VE damper should not exceed 100%, while the design maximum damper strains have been recommended to be only in the range of 60%-70% [8, 9]. Other researches concerning the performance of VE damper mostly focused on the frequency- and temperature-dependence problems encountered in the low strain phase [4, 10], whereas VE damper tends to exhibit large VE nonlinearity when the strain exceeds 100% [11]. However, there has been much less research on strain dependence of VE damper in the experimental studies as compared with other two factors.

Most of the existing mathematical models therefore only reflect the sensitivity of temperature and frequency on the performance of VE damper [4, 12, 13], models that are capable of describing the strain-dependence of VE damper are relatively few [14, 15]. Among them, the model proposed in [16] was based on the direct regression fitting of experimental results with a limited applicability for general large strain conditions. Models proposed in [15] and [14] involved very complex expressions with several coefficients, and required numerous test data. The use of finite element models, on the other hand, is computationally costly for large-scale structural modelling and analysis [17].

Due to the lack of test data under large-strain state and suitable mathematical model of VE damper, the mechanical nonlinearity of the VE damper system is usually ignored in the dynamic analysis of VE structures. For example, as an earlier study on the seismic response of VE structures, [18] assumed that the equivalent stiffness and equivalent damping of VE dampers in structure remain constant, and the design procedure proposed did not consider the effects of nonlinearity either. Many follow-up studies with reference to this method also completely ignored this factor [8, 10, 19]. In other papers focusing on the dynamic characteristics of VE structures, this influence factor is also rarely considered [4, 9].

Although ignoring the mechanical nonlinearity helps simplify the calculation process and brings convenience to the practical application of VE damper, it also introduces errors in the analysis results, leading to some unpredictable risks to the safety of structures. In addition, in the collapse analysis or pushover analysis of damped structures, large displacement often occurs. Coupled with the coupling effect of temperature and loading frequency, the viscoelastic dampers equipped in structure may show complex mechanical characteristics, and ultimately affect its damping effect in the structural level. Therefore, it is of practical significance to study the nonlinear mechanical performance of viscoelastic damper, as well as its effects on the seismic responses of viscoelastically damped structure. At present, there are only a few studies in the literature that involved such nonlinearity. For example, [20] found that the dynamic properties of a system were significantly influenced by the nonlinearity of the VE damper for seismic events. [21] presented a method to model the nonlinear responses of VE structures with a proposed extended recursive parameter model. In this way, the mechanical nonlinearity is considered, but considerable computing resource is required due to the complex calculation process. Moreover, no study has been reported emphasizing on the change of the seismic responses of VE structures caused by mechanical nonlinearity.

The main purpose of this paper is to present a mathematical model with simple expressions to describe the nonlinear mechanical behaviour of VE dampers, and develop an approximate procedure to consider such mechanical nonlinearities in the dynamic analysis of VE structures. The effects of mechanical nonlinearity on the seismic responses of VE structure are then discussed with some concluding remarks being given.

2 Mathematical model of VE damper

2.1 Model establishment

The fractional Kelvin model, which is obtained by replacing the dashpot with a fractional element, as shown in Fig. 1, is one of the simplest forms of the fractional model.

In the above model, the elasticity of VE material is expressed by the spring, and the viscosity is described through the fractional element, which can be described as [22]

$$\begin{cases} G_1 = p + q\omega^r \cos(r\pi/2) \\ \eta = \dfrac{q\omega^r \sin(r\pi/2)}{p + q\omega^r \cos(r\pi/2)} \end{cases} \tag{1}$$

where G_1 and η are the storage modulus and loss factor respectively. p and q are material coefficients of VE material corresponding to the spring element and viscosity element, ω is the excitation frequency, r is the order of the fraction with the value of $0 \leq r \leq 1$. Moreover, studies have revealed that the effect of temperature on VE material can be equivalently considered as that of frequency [23, 24], which can be expressed as

$$\begin{cases} G_1(\omega, T) = G_1(\alpha_T \omega_0, T_0) \\ \eta(\omega, T) = \eta(\alpha_T \omega_0, T_0) \end{cases} \tag{2}$$

where T are the target temperature, $\alpha_T = 10^{-12(T-T_0)/[525+(T-T_0)]}$ [4], is the temperature transformation coefficient. T_0 is the reference temperature and ω_0 is the corresponding circular frequency.

For polymer materials, the molecular chains in the matrix can be roughly assumed as elastic network chain and free network chain [25]. Elastic network chains refer to the molecular chains with complex network structure, and has a strong correlation with the elastic properties of the matrix. The free network chains are mainly those with weak interaction, non-cross-linking chains, and the side chains, which contribute to the viscosity of the matrix [26]. During the deformation process, the input energy can be consumed by the deformation and inner friction of molecular chains. However, once the deformation gets large, the chemical bonds between the molecular chains can be destroyed, dismounting the elastic network chain structure, as shown in Fig. 2. As a result, the number of elastic network chains will decrease with the increase of free network chains.

To describe these changes inside molecular chains of VE material at large strain, we here introduce two new inner variables, λ_1 and λ_2, to make an amendment to p and q for considering the variation of elasticity and viscosity of VE material simply, which is

$$\begin{cases} p = p_0 \lambda_1 \\ q = q_0 \lambda_2 \end{cases} \tag{3}$$

Where p_0 and q_0 are the reference constants at T_0. λ_1 and λ_2 are two correction factors that are used for reflecting changes of the number of elastic network chains and free network chains as well as their influences on the mechanical behaviours of VE material. To simplify the calculation, a linear relationship is adopted here to represent the correlations between the correction factors and the maximum strain $\gamma_{\max}$ [23, 24] given by equation (4).

$$\begin{cases} \lambda_1 = 1 - \kappa_1(\gamma_{\max} - \gamma_0) \\ \lambda_2 = 1 + \kappa_2(\gamma_{\max} - \gamma_0) \end{cases} \tag{4}$$

Where κ_1 and κ_2 are two modified coefficients corresponding to λ_1 and λ_2, γ_0 is a reference strain beyond which the effect of strain on the elasticity and viscosity becomes significant. For typical VE material γ_0 is around 1.0 [11]. Substituting equation (2)-(4) with $\gamma_0 = 1$ into equation (1) yields:

$$\begin{cases} G_1 = p_0\big(1 - \kappa_1(\gamma_{\max} - 1)\big) + q_0\big(1 + \kappa_2(\gamma_{\max} - 1)\big)\alpha_T\omega^r \cos(r\pi/2) \\ \eta = \dfrac{q_0\big(1 + \kappa_2(\gamma_{\max} - 1)\big)\alpha_T\omega^r \sin(r\pi/2)}{p_0\big(1 - \kappa_1(\gamma_{\max} - 1)\big) + q_0\big(1 + \kappa_2(\gamma_{\max} - 1)\big)\alpha_T\omega^r \cos(r\pi/2)} \end{cases} \tag{5}$$

Equation (5) is the modified equivalent fractional Kelvin model with six independent coefficients, p_0, q_0, T_0, κ_1, κ_2, r.

2.2 Experimental evaluation of mechanical properties on VE dampers

A series of experiments have been carried out on three identical VE dampers under different strain, temperature, and frequency conditions. The VE damper specimens were classical sandwich-type samples consisting of two VE material layers with 10mm thickness for each layer, and the area of the VE material layer was 3000 mm^2. The actual test setup is shown in Fig. 3.

The experiment protocols are listed in Table 1. All specimens were subjected to sinusoidal loads. To avoid the probable damage caused by continuously loading under multiple conditions, the experimental specimens were divided into two groups for specific working conditions. Group 1 was used for the identification of model parameters, and group 2 was employed for model validation.

Fig. 4 shows the measured hysteresis curves of VE dampers under different strain conditions. The hysteretic curves exhibit a standard elliptic shape when strains are less than 50%, and this indicates that the mechanical properties of the damper are basically in the viscoelastic linear stage. As the strain approaches 100%, the slope of the hysteretic curve begins to change, the VE damper begins to behave in a nonlinear viscoelasticity manner. With further increase of the strain, the nonlinear viscoelasticity characteristics of VE damper become more pronounced, indicating that the VE damper has entered an abnormal working region. The shape of the hysteretic curve has changed from an ellipse to an inverse S-shaped curve.

The storage modules G_1 and loss factor η are often employed for a quantitative description of the stiffness and energy dissipation of VE materials, calculated by

$$G_1 = \frac{F_1 h_v}{n_v A_v u_0} \tag{6}$$

$$\eta = \frac{F_2}{F_1} \tag{7}$$

where F_1 and F_2 are the corresponding force at the maximum displacement u_0 and zero displacement respectively, n_v is the number of VE layers, A_v and h_v are the shear area and thickness of the VE layer. For the tested VE damper specimens, the corresponding G_1 and η under different strains are calculated and the results are shown in Table 2 and Fig. 5.

It can be seen that the mechanical properties of VE dampers show a trend of degradation with increase of the strain, and the degradation rate of the two indicators in the normal working region is much lower than that in the abnormal working region. G_1 and η have a reduction of 13.8 % and 17.9% with the maximum strain increasing from 50% to 100%, while the reduction values increased to 61.2% and 29.8% with max maximum strain raising from 150% to 200%. This is because the previous damage generated inside the VE material is accumulated in the damage process of the molecular chain structure, and aggravates the later damage process afterward. Therefore, the whole degradation process of the energy dissipation capacity of VE material exhibits acceleration, and this also suggests that the strain state has a remarkable effect on the mechanical properties of the VE damper.

From the experiments, it was also observed that shear failure occurred to the material layer when the strain was very large, leading to the destruction of the VE damper, as shown in Fig. 6.

2.3 Model parameter determination and model validation

The coefficients of the proposed model were determined by MATLAB with the genetic algorithm. The objective function χ^2 used in the fitting process is set as

$$\chi^2 = \sum_{i=1}^{n_{\text{test},1}} \left(G_{1,cal}\left(\omega^i, T^i, \gamma_{max}^i, \phi\right) - G_{1,test}^i\right)^2 + \sum_{i=1}^{n_{\text{test},2}} \left(\eta_{cal}\left(\omega^i, T^i, \gamma_{max}^i, \phi\right) - \eta_{test}^i\right)^2 \tag{8}$$

Where ω^i, T^i, γ_{max}^i, $G_{1,test}^i$, $\eta_{1,test}^i$, are the test values of the measured excitation frequencies, ambient temperatures, storage modulus and loss factor, respectively, and the superscript i represents the i$^{\text{th}}$ test value. $G_{1,cal}\left(\omega^i, T^i, \gamma_{max}^i, \phi\right)$ and $\eta_{1,cal}(\omega^i, T^i, \gamma^i, \phi)$ are the corresponding calculations of the proposed model for storage modulus and loss factor. $n_{\text{test},1}$ and $n_{\text{test},2}$ are the test number of the storage modulus and loss factor. ϕ is the vector of the undetermined parameters of the proposed model, which is.

$$\phi = (p_0, q_0, T_0, \kappa_1, \kappa_2, r)^{\text{T}} \tag{9}$$

Following the above procedure, the parameters of three models for the test VE damper specimens were determined, as shown in Table 3.

To illustrate the accuracy of the proposed model, the model with the identified parameter values is used to predict the test results for the 2$^{\text{nd}}$ group of specimens. For comparison, the equivalent fractional kelvin model and the equivalent standard solid model [4, 27] (hereinafter referred to as Model 1 and

Model 2) are also employed to perform the respective predictions. The calculation results of three models are listed in Table 4.

Fig. 7 (a), (d) presents the predicted results of three models under different strains. It can be seen that the prediction accuracy of the proposed model under different strain states is better than these of model 1 and model 2 overall, and its relative errors are within the 20% as compared to 57.1% and 49.7% for model 1 and 2, respectively. Besides, with the strain reaching the abnormal working region, model 1 and model 2 tend to show increased prediction errors; the maximum prediction error for G_1 and η respectively reaches 59.4% and 39.4% for model 1, 49.7% and 47.8% for model 2, and reduces to18.3% and 19.0% using the proposed modified model.

Fig. 7 (b), (e) and Fig. 7 (c), (f) show the comparison of results under different frequencies and temperatures. It can be seen that all these three models approximately show similar prediction accuracy under different frequencies with errors all within a limit of 20%, the prediction accuracy of these three models for G_1 is better than that for η, and this is because the magnitude of loss factor is smaller than that of storage modulus, therefore η tends to be more sensitive to the prediction error. As for the effects of temperature, all three models predict very well the storage modulus G_1, while the proposed model exhibits the best prediction accuracy for the loss factor η, especially under low-temperature conditions.

3 Approximate method for considering mechanical nonlinearity in seismic analysis of VE structures

For a dynamic system, the equation of motion can be written as

$$\mathbf{M}\ddot{X} + C_s\dot{X} + K_sX = -\mathbf{MI}\ddot{X}_g \tag{10}$$

After installing the VE damper system, the equation of motion is modified as

$$\mathbf{M}\ddot{X} + (C_s + C_d)\dot{X} + (K_s + K_d)X = -\mathbf{MI}\ddot{X}_g \quad (11)$$

where $\mathbf{M}$ is the mass matrix; X, $\dot{X}$, and $\ddot{X}$ are systematic displacement, velocity, and acceleration; C_s and K_s are the modal damping matrix and stiffness matrix of the system; $\mathbf{I}$ is the unit vector; $\ddot{X}_g$ is the ground motion acceleration; C_d and K_d are the equivalent damping matrix and equivalent stiffness matrix of VE dampers respectively, which can be determined by the equivalent model [18].

Taking the effects of excitation frequency, strain amplitude and working temperature into consideration, the equivalent model can be rewritten as

$$\begin{cases} K_d = \dfrac{n_v A_v}{h_v} G(T, \omega, \gamma_{\max}) \\ C_d = \dfrac{K_d}{\omega} \eta(T, \omega, \gamma_{\max}) \end{cases} \quad (12)$$

For a general situation, T, ω, and $\gamma_{\max}$ may change constantly during the dynamic response, so C_d and K_d need to be determined accordingly, and the VE dynamic system represented by equation (11) can then be solved by the time-stepping method. For seismic response analysis, because the duration of an earthquake is short, the temperature of VE damper can be assumed as constant in the loading process. To consider the strain dependency, the maximum strain of VE damper that has been reached up to the j th integration step is taken for the calculation in the j+1 th integration step, thus equation (12) can be written in the numerical form as

$$\begin{cases} K_d^{j+1} = \dfrac{n_v A_v}{h_v} G_1^{j+1}(T, \omega, \gamma_{\max}^j) \\ C_d^{j+1} = \dfrac{K_d^{j+1}}{\omega} \eta^{j+1}(T, \omega, \gamma_{\max}^j) \end{cases} \quad (13)$$

where the superscript represents the corresponding integration step. After a small initial strain of VE damper is given, C_d and K_d of VE damper at each integration step can be calculated by iteration.

The seismic wave usually exhibits a time-varying characteristic of frequency, the instantaneous frequency (IF) is adopted here to describe the characteristics of seismic frequency. For signal $s(t)$, the time-frequency ridge $\tilde{f}_i(t)$ refers to the peak frequency at each time in its time-frequency distribution $TFR_s(t,f)$, as

$$\tilde{f}_i(t) = \arg[\max TFR_s(t,f)] \tag{14}$$

On the time-frequency surface, the energy of the signal is always concentrated along with the IF. The corresponding frequency of the time-frequency ridge of the signal is equal to or approximately equal to the IF of the signal itself [28, 29]. Generally speaking, a signal can be regarded as the superposition of several main components with particular frequency parameters, and the signal component with high energy often plays a dominant role in the change of whole signal. Therefore, the IF of the time-frequency ridge of the signal component with the highest energy can approximately be taken as the parameter to describe the frequency of the target signal.

To identify the IF, the Wavelet transformation (WT) method is often employed, expressed in a general form as [30]

$$WT_s(\tau,a) = \frac{1}{\sqrt{a}}\int_{-\infty}^{+\infty} s(t)\psi^*(\frac{t-\tau}{a})\,dt \tag{15}$$

where ψ is mother wavelet function; * means conjugate; and a and τ are scale parameter and shift parameters. The WT method is adopted here to obtain the time-frequency characteristics of the seismic ground motion, and the IF of the ground motion signal is then traced [31, 32].

The Wavelet analysis toolbox of MATLAB is used to analyse the time-frequency contents. For the 1940 El Centro wave, its IF is calculated as shown in the red line in Fig. 8. It can be seen that the IF of the El Centro wave changes all the time within a range of 0~10Hz.

When the IF of the seismic load is determined, the effects of the seismic frequency on the dynamic properties of VE dampers can be considered by substituting the corresponding frequency into Equation (11) at each integration step. Equation (13) is then updated to

$$\begin{cases} K_d^{j+1} = \dfrac{n_v A_v}{h_v} G_1^{j+1}(T, \omega^{j+1}, \gamma_{\max}^j) \\ C_d^{j+1} = \dfrac{K_d^{j+1}}{\omega^{j+1}} \eta^{j+1}(T, \omega^{j+1}, \gamma_{\max}^j) \end{cases} \tag{16}$$

Based on the proposed method, dependences between the performance of VE dampers in the structure and temperature, strain, frequency can be approximately taken into account in the calculation process, and the seismic response of VE structure considering mechanical nonlinearity can be calculated through equation (5), (11) and (16) by iteration.

4 Effects of mechanical nonlinearity on the seismic responses of VE structures

To quantitatively study the influence of mechanical nonlinearity on the seismic response of a VE damped system, two different VE shear frames are taken to conduct the numerical analysis, as shown in Fig. 9, which represent the proportionally damped case and non-proportionally damped case, respectively.

4.1 The proportionally damped frame

The proportionally damped frame is a flexible moment-resistant frame with a uniform story height of 2.7m. The stiffness and mass of VE structure are assumed to be k =1.8×10^3 KN/m and m = 6000 kg respectively. Fig. 10 (a) shows the first three mode shapes and natural frequencies. For simplification, the Rayleigh damping is employed in the following analysis with assuming that the first and third modal damping ratios are 2%.

In engineering, the mechanical nonlinearity is often ignored for the convenience of calculation, C_d and K_d with fixed values measured at nominal strain and frequency are determined as the stiffness contribution and damping contribution of the VE dampers in the design and analysis process [4, 13]. To reveal the difference of the seismic responses of VE structure with and without considering such mechanical nonlinearity, the nominal design temperature, the nominal design frequency, and the nominal design strain of the VE dampers are set as 18°C, 0.79 Hz, and 0.2 with the shear layer of 0.001m for the VE damper in the following numerical examples. The 1st order modal damping ratio is designed as 12.5% for the VE damped structures. Three earthquake ground motions, namely El Centro, Taft, and an artificial earthquake, are selected as the seismic excitation and the Wilson-θ method is employed for the numerical integration in this paper. To make the numerical results comparable, the maximum accelerations of the three records are adjusted to 3.0m/s^2.

Fig. 11 show the displacement and acceleration response time histories of the above three structure scenarios at the roof level under different earthquake ground motions. Fig. 12 present a comparison of the lateral displacement envelope and the inter-story drift envelope, respectively. The corresponding maximum structural responses are listed in Table 5.

It can be seen from Fig. 11 that the maximum roof displacement and acceleration under different earthquake excitations are reduced considerably by installing the VE damper system. Under the El Centro ground motion, the maximum roof displacement and acceleration of the uncontrolled structure are 20.92 mm and 4.87 m/s^2, while the corresponding VE structure (when ignoring the viscoelastic nonlinear effect) are only 2.42 mm and 0.85 m/s^2, respectively, with the reduction rate of 88.4% and 82.5%. Besides, the story drift and the lateral displacement of the uncontrolled structure are also far greater than those of the VE structure, as shown in Fig. 12. The maximum story drift of the uncontrolled structure is 0.6%, which exceeds the limitation of 0.4% in the current code [33]. After adding the VE dampers, the value is reduced to 0.08% with a reduced rate of about 85%. Similar trend can be observed under the other two earthquakes.

Comparing the seismic responses of VE structure with and without considering the mechanical nonlinearity, it can be found that ignoring the nonlinearity results in a marked underestimation of the seismic response for the VE structure. The maximum roof displacement of the VE structure without considering the mechanical nonlinearity under El Centro, Taft, and the artificial earthquake ground motions are 7.09 mm, 4.61 mm, and 4.04 mm, respectively, whereas the corresponding structural responses considering the mechanical nonlinearity are 2.42 mm, 4.05 mm, and 2.79 mm. In other words, without considering the mechanical nonlinearity leads to an underestimation of the roof displacement of 65.9%, 12.1%, and 30.9% under the three ground motions, respectively. Regarding the roof acceleration, the underestimation becomes 63.4%, 59.2% and 60.4%, respectively. In terms of the lateral displacement envelope and story drift envelope of the VE structure, the comparative trend is similar. The maximum lateral drift is found to be 0.090%, 0.074% and 0.059% for El Centro, Taft, and the artificial ground motions without considering the mechanical nonlinearity, and 0.14%, 0.09%, and 0.08% with considering the nonlinearity. This suggests that the maximum story drift may not actually meet the design requirements when the mechanical nonlinearity is taken into account in some cases, even if it was satisfied in the design process without considering the mechanical nonlinearity.

As mentioned in Section 3, due to the dynamic characteristics of ground motions, the strain and frequency of the VE damper change constantly during the loading process. Taking VE damper at the first floor as an example, Fig. 15 (a) shows the time histories of the damping force in the VE damper at the first floor, and Table 7 lists its corresponding Max damping force. It can be observed that, in most cases, the force in the VE damper computed without considering the nonlinearity is greater than that when the nonlinearity is taken into account. The max damping forces of VE damper in 1floor are 12.72 KN, 9.08 KN, and 8.68 KN under El Centro, Taft, and the artificial earthquake ground motions when neglecting nonlinearity, and change to 12.26 KN, 7.27 KN, and 7.32 KN after considering nonlinearity, with the average change rate of 13.1%. Fig. 16 (a) presents the hysteresis curves of VE damper under three earthquake ground motions, respectively. As can be seen, the actual strain experienced by the VE damper constantly changes, leading to the considerable variation of the energy-dissipation capacity and stiffness of VE damper. In other words, ignoring the nonlinear characteristics of the VE dampers could lead to serious misestimation of the structural resistance, resulting in unsafe design.

4.2 The non-proportionally damped frame

The non-proportionally damped frame is a ten-story steel frame with VE dampers installed in eight floors at the bottom of the structure, shown in Fig. 9 (b). The structural information of this steel frame is form in [34]' study. The nominal design frequency of VE dampers are set as 0.46 Hz according to the mode information of the structure, the 1st order modal damping ratio is designed as 9.09% with other design parameters keeping consistent with that in Section 4.1. Besides, the same earthquake ground motions and numerical integration strategy are employed here. The first three mode shapes and natural frequencies are shown in Fig. 10 (b).

Fig. 13 exhibits the roof displacement and roof acceleration response time histories of the non-proportionally damped structure under three earthquake ground motions. Fig. 14 present the lateral displacement envelope and the inter-story drift envelope at three structure scenarios, respectively. The corresponding maximum structural responses are listed in Table 6.

As can be seen from Fig. 13 and Fig. 14, the installation of VE dampers significantly reduces the seismic responses of the non-proportionally damped structure. Taking the El Centro case as an example, the maximum roof displacement and acceleration of the uncontrolled structure are reduced from 12.50 mm and 2.10 m/s^2 to 3.36 mm and 0.40 m/s^2 (when ignoring the viscoelastic nonlinear effect) by installing the VE damping system, respectively, with the reduction rate of 73.1% and 81.0%. Regarding the story drift and the lateral displacement, the reduced rates has been reduced by 80.7%, suggesting that the VE damper system possesses excellent vibration-control capacity.

Besides, it can be concluded that the influence of the mechanical nonlinearity of VE dampers on the seismic responses of the non-proportionally damped frame is similar to that of the proportionally damped frame. The maximum roof displacement of the non-proportionally damped VE structure without considering the mechanical nonlinearity under El Centro, Taft, and the artificial earthquake ground motions are 3.36 mm, 2.41 mm, and 1.36 mm, respectively, whereas the corresponding structural responses considering the mechanical nonlinearity are 5.30 mm, 3.93 mm, and 2.35 mm. Namely, neglecting such mechanical nonlinearity leads to the underestimation of the structural responses by 36.6%, 38.6%, and 42.1% under above three earthquakes. In terms of the roof acceleration, the underestimation becomes 39.4%, 50.0% and 51.4%, respectively. Moreover, it can also be observed that the maximum lateral drift changes from 0.074%, 0.041% and 0.032% to 0.123%, 0.085%, and 0.070% after considering the mechanical nonlinearity under El Centro, Taft, and the artificial ground motions. As for the lateral displacement envelope, the comparative trend is similar. It can be concluded from the above analysis that the influence of such mechanical nonlinearity on the structural seismic response of proportionally and non-proportionally damped system is similar, that is, the structural responses increases can be underestimated when the mechanical nonlinearity is not considered, which is not safe to the performance evaluate of the structure.

Fig. 15 (b) and Fig. 16 (b) show the time histories of the damping force and the hysteresis curves of the VE damper at the first floor, Table 7 lists the corresponding max damping force. As can be seen, the influence of the mechanical nonlinearity on the mechanical behaviour of VE dampers in the non-proportionally damped case is similar to that of proportionally damped case. The max damping forces of VE damper in 1floor are 24.19 KN, 15.01 KN, and 17.63 KN under El Centro, Taft, and the artificial earthquake ground motions when neglecting nonlinearity, and change to 15.90 KN, 11.75 KN, and 12.24 KN after considering nonlinearity, with the average change rate of 28.9%. The damping capacity of the VE damper can be significantly overestimated by neglecting the nonlinearity in both the proportional and non-proportionally damped frames.

5 Concluding remarks

In this paper, a modified equivalent fractional Kelvin model is proposed to represent the mechanical nonlinearity of VE damper. The model parameters are determined experimentally and comparatively. The effects of mechanical nonlinearity on the seismic responses of VE structure are discussed. The following conclusions are made:

(1) Verification suggests that the proposed model is capable of describing the energy dissipation and stiffness characteristics of VE damper in a wide temperature and frequency range, and it also has a high prediction accuracy under large strains.

(2) Experiments on VE dampers showed that with the increase of strain level, the damage accumulation accelerated due to the irreversible damage of the molecular chain structure, the energy dissipation capacity and stiffness of VE damper showed a degradation trend, and the degradation rate tends to be higher in the normal working stage than that in the larger strain stage.

(3) An approximate method for calculating the seismic responses of VE structure with considering the mechanical nonlinearity of the VE damper system is proposed. The seismic responses of the representative VE structures with and without considering such nonlinearity are then calculated and compared in the proportionally and non-proportionally damped cases, respectively. The comparative results demonstrate that the peak seismic responses of a VE structure tend to be markedly underestimated when the mechanical nonlinearity of VE damper is ignored.

(4) Although the quantitative effects may vary for different characteristics of structures and the seismic excitations, it may be generally concluded that the mechanical nonlinearity plays a significant role in the performance of VE dampers, and consequently affects the seismic response of structures equipped with VE dampers. It is therefore deemed necessary to consider the mechanical nonlinearity of VE

dampers in the design and performance evaluation of the VE structures, especially in the large-strain conditions.

Acknowledgments

The authors acknowledge financial supports for this research from The National Key Research and Development Program of China (2016YFE0200500), National Science Fund for Distinguished Young Scholars (51625803), Program of Chang Jiang Scholars of Ministry of Education, Ten Thousand Talent Program of Leading Technologists, Jiangsu International Science and Technology Cooperation Program (BZ2018058).

Declaration of interests

The authors declare no conflict of interest in preparing this article.

References

[1] P. Mahmoodi, L.E. Robertson, M. Yontar, C. Moy, L. Feld, Performance of Viscoelastic Dampers in World Trade Center Towers, American Society of Civil Engineers, (2015).

[2] R.H. Zhang, T.T. Soong, Seismic Design of Viscoelastic Dampers for Structural Applications, Journal of Structural Engineering, 118 (1992) 1375-1392.

[3] Y.R. Dong, Z.D. Xu, Q.Q. Li, Y. S. Xu, Z. H. Chen, Seismic behavior and damage evolution for retrofitted RC frames using haunch viscoelastic damping braces, Engineering Structures, 199 (2019) 109583.

[4] Z.D. Xu, C. Xu, J. Hu, Equivalent fractional Kelvin model and experimental study on viscoelastic damper, Journal of Vibration and Control, 21 (2013) 2536-2552.

[5] R.D.A. De Lima A M G, Lacerda H B, et al, An investigation of the self-heating phenomenon in viscoelastic materials subjected to cyclic loadings accounting for prestress, Mechanical Systems and Signal Processing, (2015).

[6] P. Cassagnau, F. Mélis, Non-linear viscoelastic behaviour and modulus recovery in silica filled polymers, Polymer, 44 (2003) 6607-6615.

[7] F. Petrone, M. Lacagnina, M. Scionti, Dynamic characterization of elastomers and identification with rheological models, Journal of Sound and Vibration, 271 (2004) 339-363.

[8] R.H. Zhang, T.T. Soong, P. Mahmoodi, Seismic response of steel frame structures with added viscoelastic dampers, Earthquake Engineering and Structural Dynamics, 18 (2010) 389-396.

[9] J.M. Tchamo, Z. Ying, An alternative practical design method for structures with viscoelastic dampers, Earthquake Engineering and Engineering Vibration, 017 (2018) 459-473.

[10] K.W. Min, J. Kim, S.H. Lee, Vibration tests of 5-storey steel frame with viscoelastic dampers, Engineering Structures, 26 (2004) 831-839.

[11] I.D. Aiken, Earthquake simulator testing and analytical studies of two energy-absorbing systems for multistory s, University of California, 1990.

[12] F. Mazza, A. Vulcano, Control of the earthquake and wind dynamic response of steel-framed buildings by using additional braces and/or viscoelastic dampers, Earthquake Engineering and Structural Dynamics, 40 (2011) 155-174.

[13] R. Lewandowski, M. Przychodzki, Approximate method for temperature-dependent characteristics of structures with viscoelastic dampers, Archive of Applied Mechanics, 88 (2018) 1695-1711.

[14] K. Kasai, Y. Ooki, K. Tokoro, K. Amemiya, K. Kimura, JSSI manual for building passive control technology part-9 time-history analysis model for viscoelastic dampers, in: 13th World Conf. on Earthquake Engineering, International Association of Earthquake Engineering Vancouver, Canada, 2004.

[15] S.J. Wang, I.C. Chiu, C.H. Yu, K.C. Chang, Experimental and analytical study on design performance of full-scale viscoelastic dampers, Earthquake Engineering and Engineering Vibration, 17 (2018) 693-706.

[16] K.C. Chang, T.T. Soong, S.T. Oh, M.L. Lai, Seismic Behavior of Steel Frame with Added Viscoelastic Dampers, Journal of Structural Engineering Asce, 121 (1995) 1418-1426.

[17] C.S. Tsai, Temperature Effect of Viscoelastic Dampers during Earthquakes, Journal of Structural Engineering, 120 (1994) 394-409.

[18] K. Chang, M. Lai, T.T. Soong, D. Hao, Y. Yeh, Seismic behavior and design guidelines for steel frame structures with added viscoelastic dampers, National Center for Earthquake Engineering Research Buffalo, NY, 1993.

[19] K. C. Chang, Y. Y. Lin, Seismic response of full-scale structure with added viscoelastic dampers, Journal of Structural Engineering, 130 (2004) 600-608.

[20] A. Dall'Asta, L. Ragni, Nonlinear behavior of dynamic systems with high damping rubber devices, Engineering Structures, 30 (2008) 3610-3618.

[21] A.R. Ghaemmaghami, O.-S. Kwon, Nonlinear modeling of MDOF structures equipped with viscoelastic dampers with strain, temperature and frequency-dependent properties, Engineering Structures, 168 (2018) 903-914.

[22] R. Lewandowski, B. Chorazyczewski, Identification of the parameters of the Kelvin–Voigt and the Maxwell fractional models, used to modeling of viscoelastic dampers, Computers and Structures, 88 (2010) 1-17.

[23] K. Kasai, Constitutive rule for viscoelastic materials considering temperature, frequency, and strain sensitivities, Journal of Structural and Construction Engineering, 543 (2001) 77-86.

[24] Z.D. Xu, D.X. Wang, C.F. Shi, Model, tests and application design for viscoelastic dampers, Journal of Vibration and Control, 17 (2011) 1359-1370.

[25] S. Tang, M.S. Greene, W.K. Liu, Two-scale mechanism-based theory of nonlinear viscoelasticity, Journal of the Mechanics and Physics of Solids, 60 (2012) 199-226.

[26] T. Koga, T. Hashimoto, M. Takenaka, K. Aizawa, N. Amino, M. Nakamura, D. Yamaguchi, S. Koizumi, New Insight into Hierarchical Structures of Carbon Black Dispersed in Polymer Matrices: A Combined Small-Angle Scattering Study, Macromolecules, (2008).

[27] Z.D. Xu, Experimental Study on the (Lead) Viscoelastic Structure, in, Xi'an Architecture & Technology University, China, 2001.

[28] V.N. Ivanovic, M. Dakovic, L. Stankovic, Performance of quadratic time-frequency distributions as instantaneous frequency estimators, Signal Processing IEEE Transactions on, 51 (2003) 77-89.

[29] B. Boashash, Estimating and interpreting the instantaneous frequency of a signal. II. Algorithms and applications, Proceedings of the IEEE, 80 (1992) 540-568.

[30] N. Delprat, B. Escudié, P. Guillemain, R. Kronland-Martinet, P. Tchamitchian, B. Torresani, Asymptotic wavelet and Gabor analysis: Extraction of instantaneous frequencies, IEEE transactions on Information Theory, 38 (1992) 644-664.

[31] D. Iatsenko, P.V. McClintock, A. Stefanovska, Extraction of instantaneous frequencies from ridges in time–frequency representations of signals, Signal Processing, 125 (2016) 290-303.

[32] S.A. Fulop, K. Fitz, Algorithms for computing the time-corrected instantaneous frequency (reassigned) spectrogram, with applications, The Journal of the Acoustical Society of America, 119 (2006) 360-371.

[33] MCPRC, Code for Seismic Design of Buildings (GB 50011-2010), in, China Architecture and Building Press, Beijing, 2010.

[34] J. Dai, Z.D. Xu, P.P. Gai, X. Yan, Seismic performance of viscoelastically damped structures at different ambient temperatures, Journal of Vibration and Control, 0 (2021) 1077546320966930.

Figures

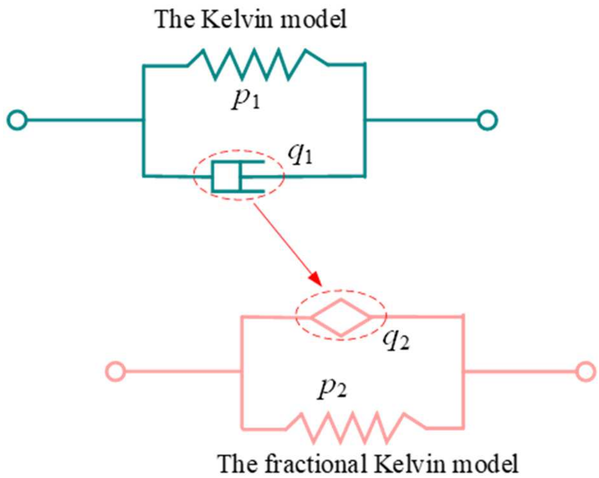

Fig. 1. Schematic of the fractional Kelvin model

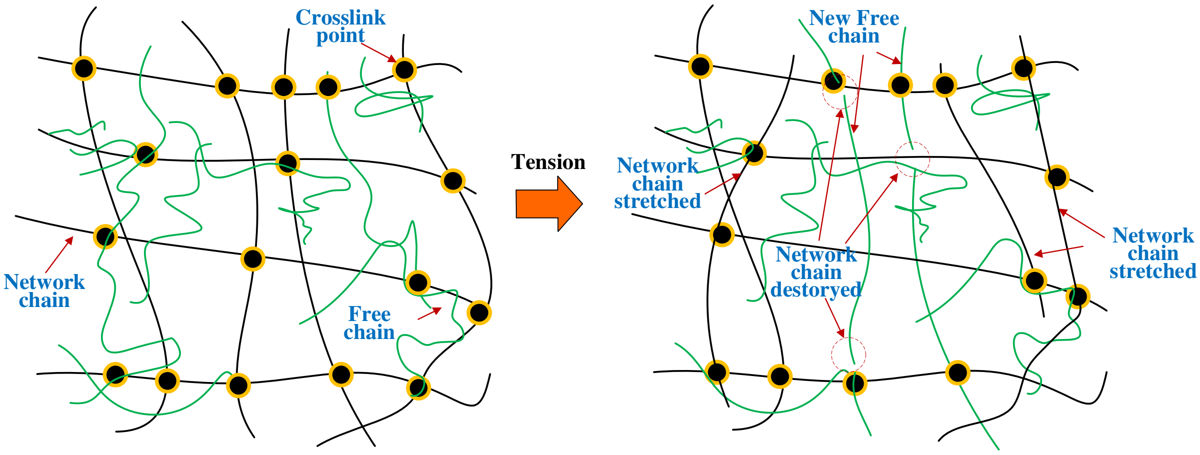

Fig. 2. Illustration of molecular chains inside VE material during deformation

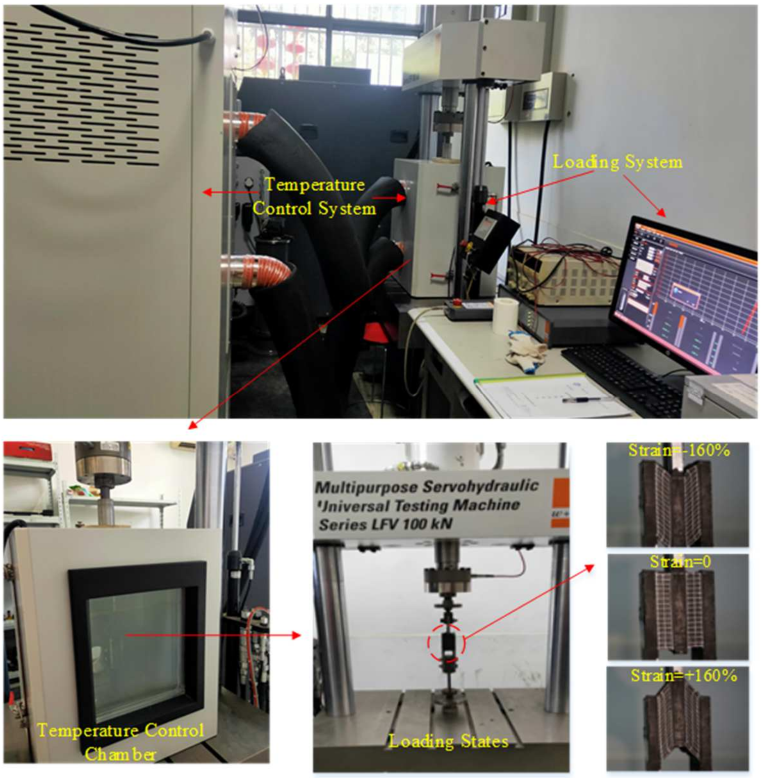

Fig. 3. Test setup for VE damper specimens

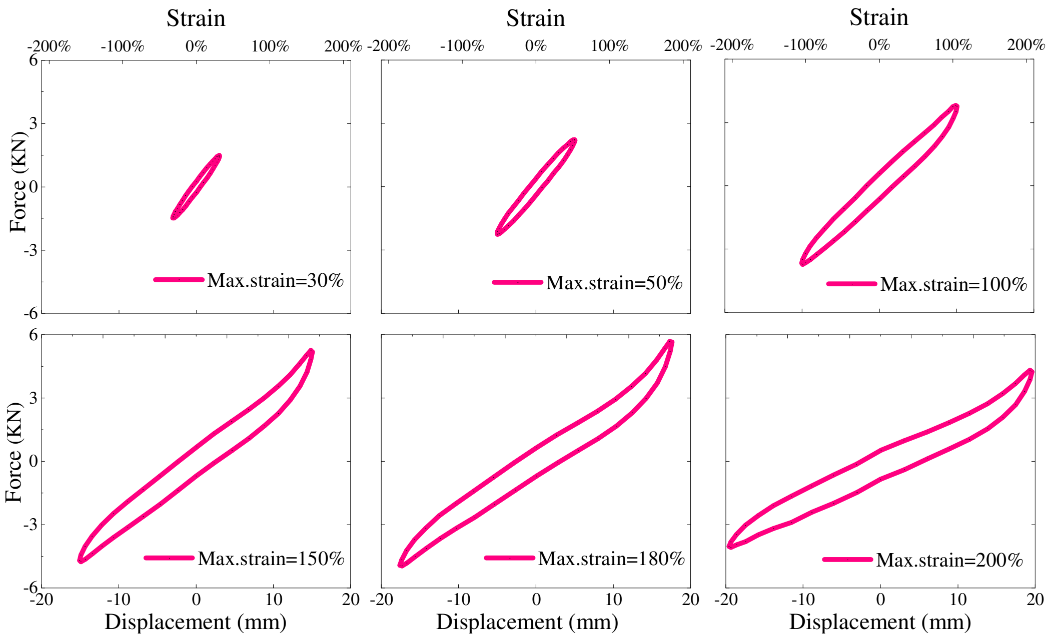

Fig. 4. Hysteresis curves of VE damper under different strain stages

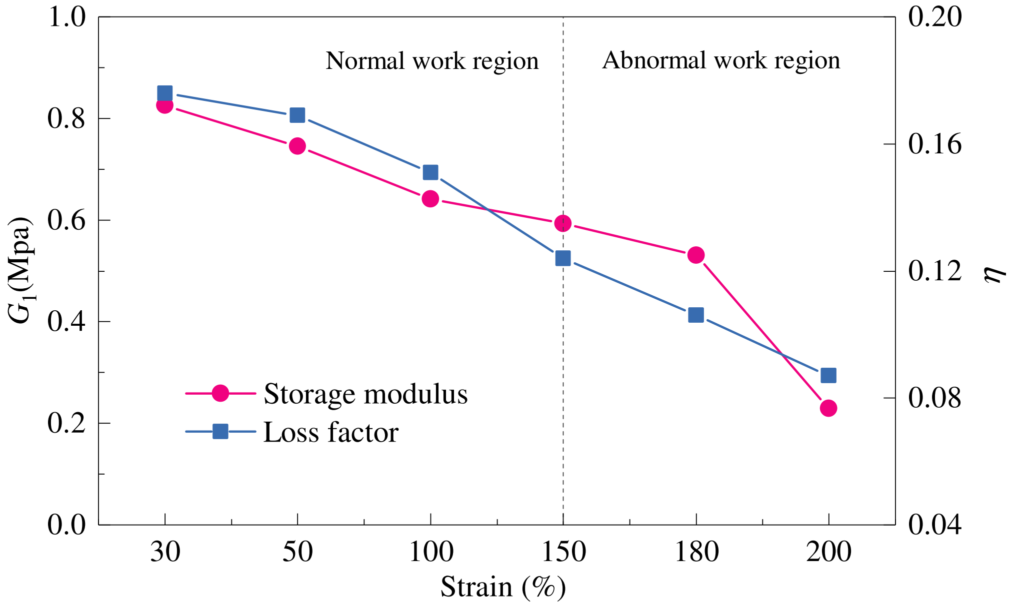

Fig. 5. G_1 and η at different strains

Fig. 6. Failure of VE dampers

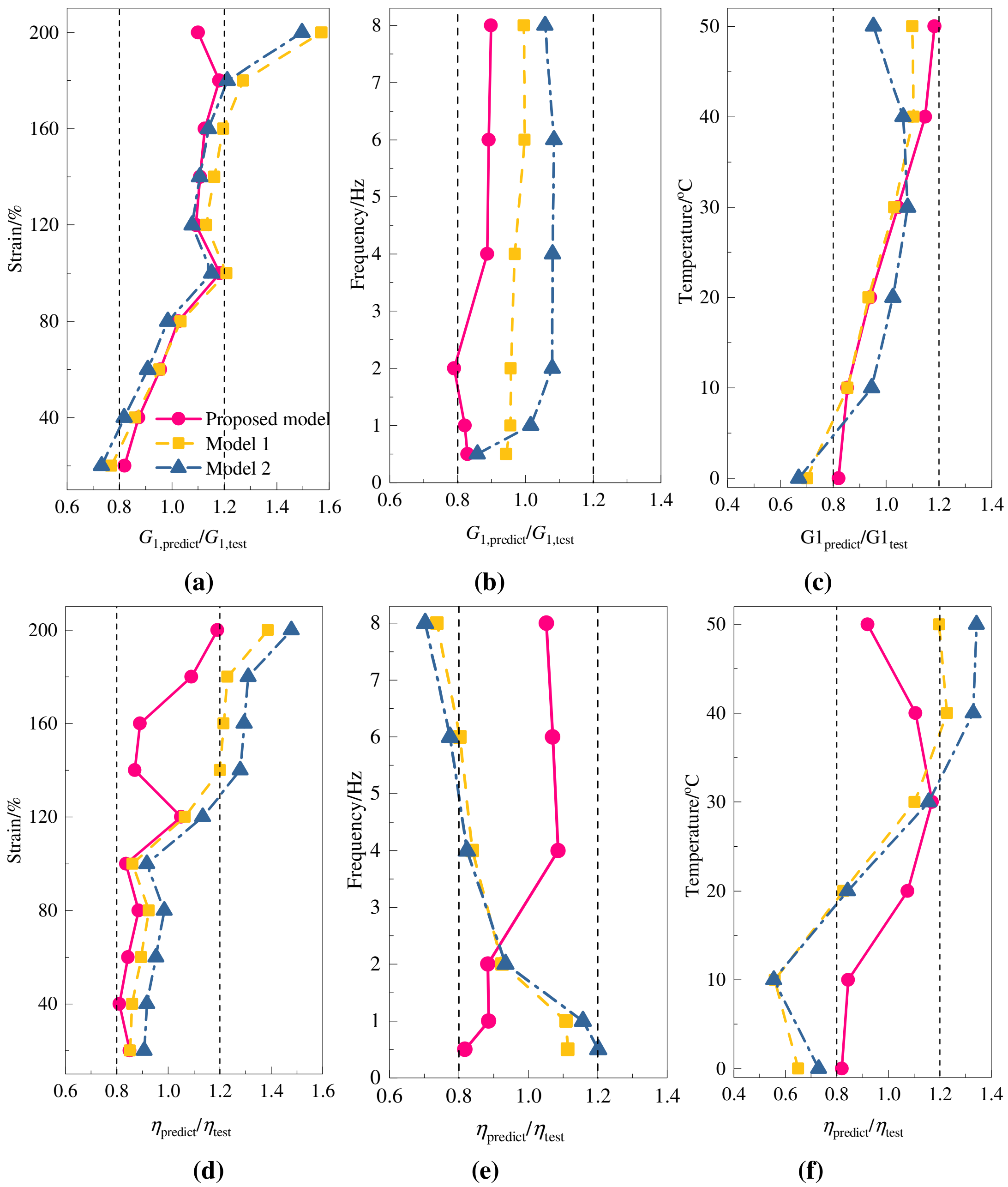

Fig. 7. Normalized prediction of G_1 and η. (a) and (d) under different strains; (b) and (c) under different frequencies; (a) and (d) under different temperatures

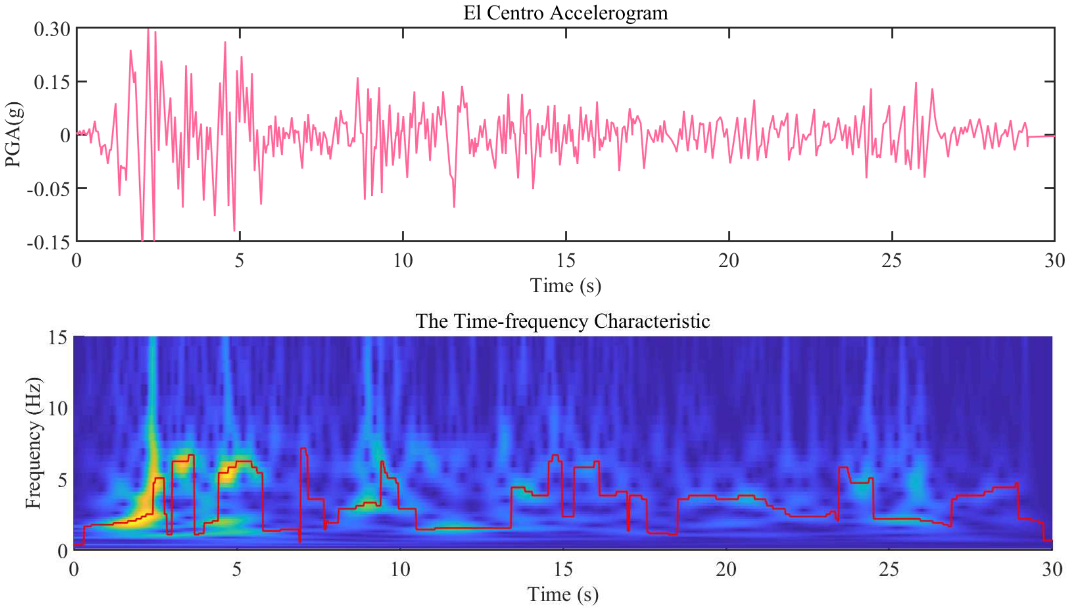

Fig. 8. IF of El Centro wave estimated by WT method

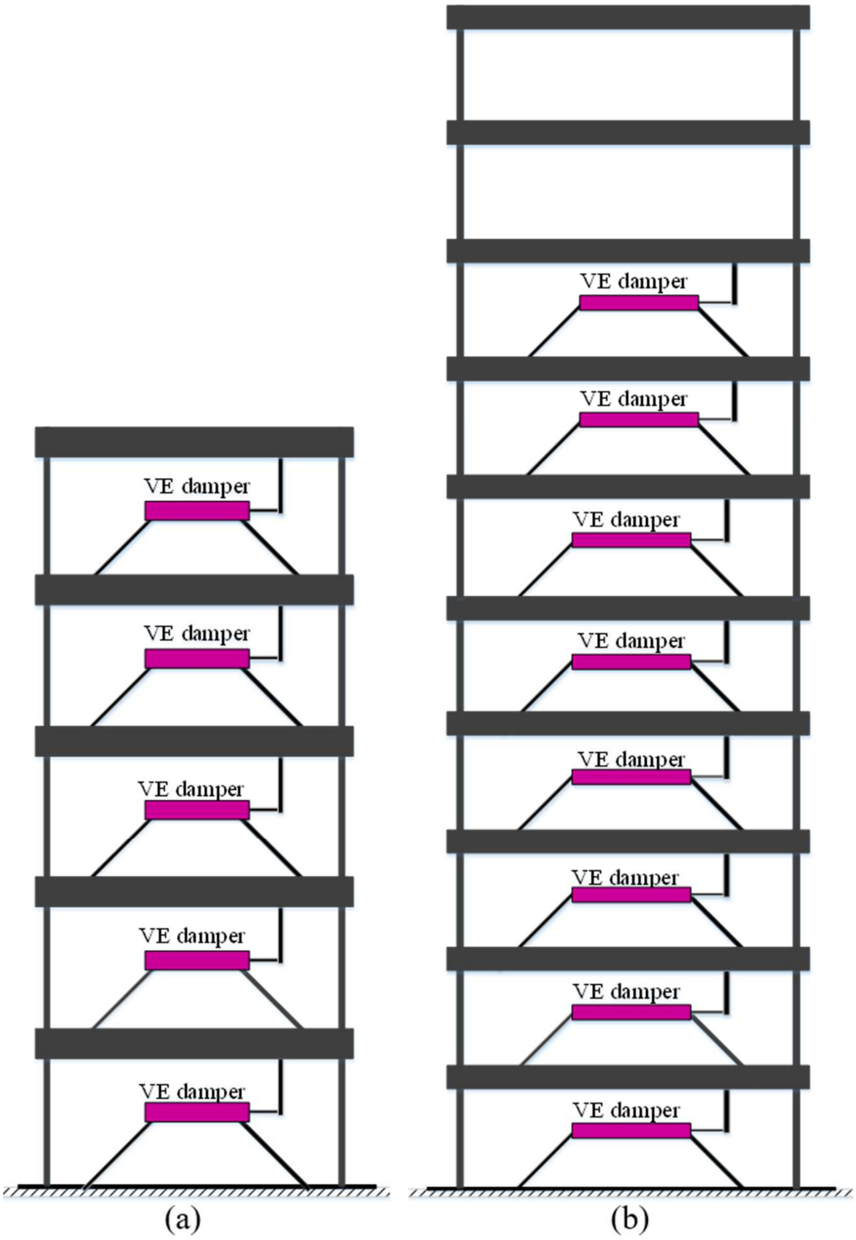

Fig. 9. VE damper structure. (a) The proportionally damped case; (b) The non-proportionally damped case.

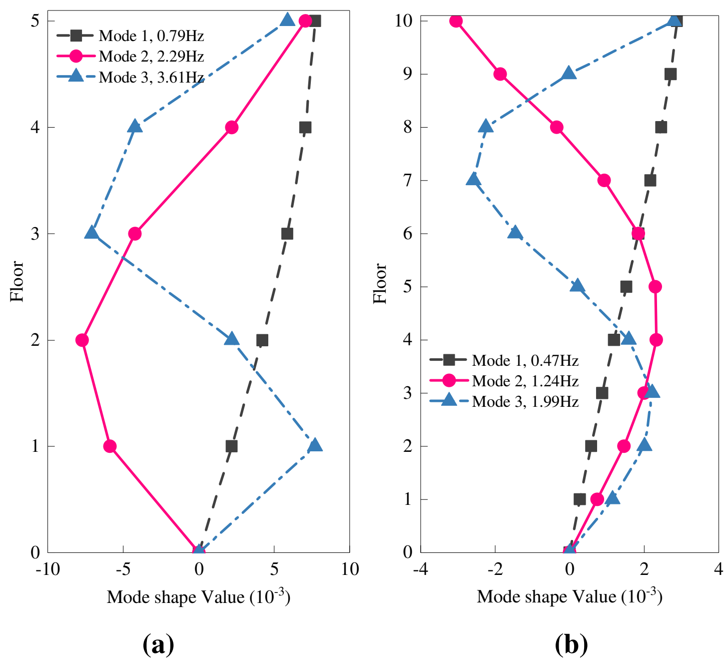

Fig. 10. First three mode shapes and natural frequencies of two numerical structures. (a) The proportionally damped case; (b) The non-proportionally damped case.

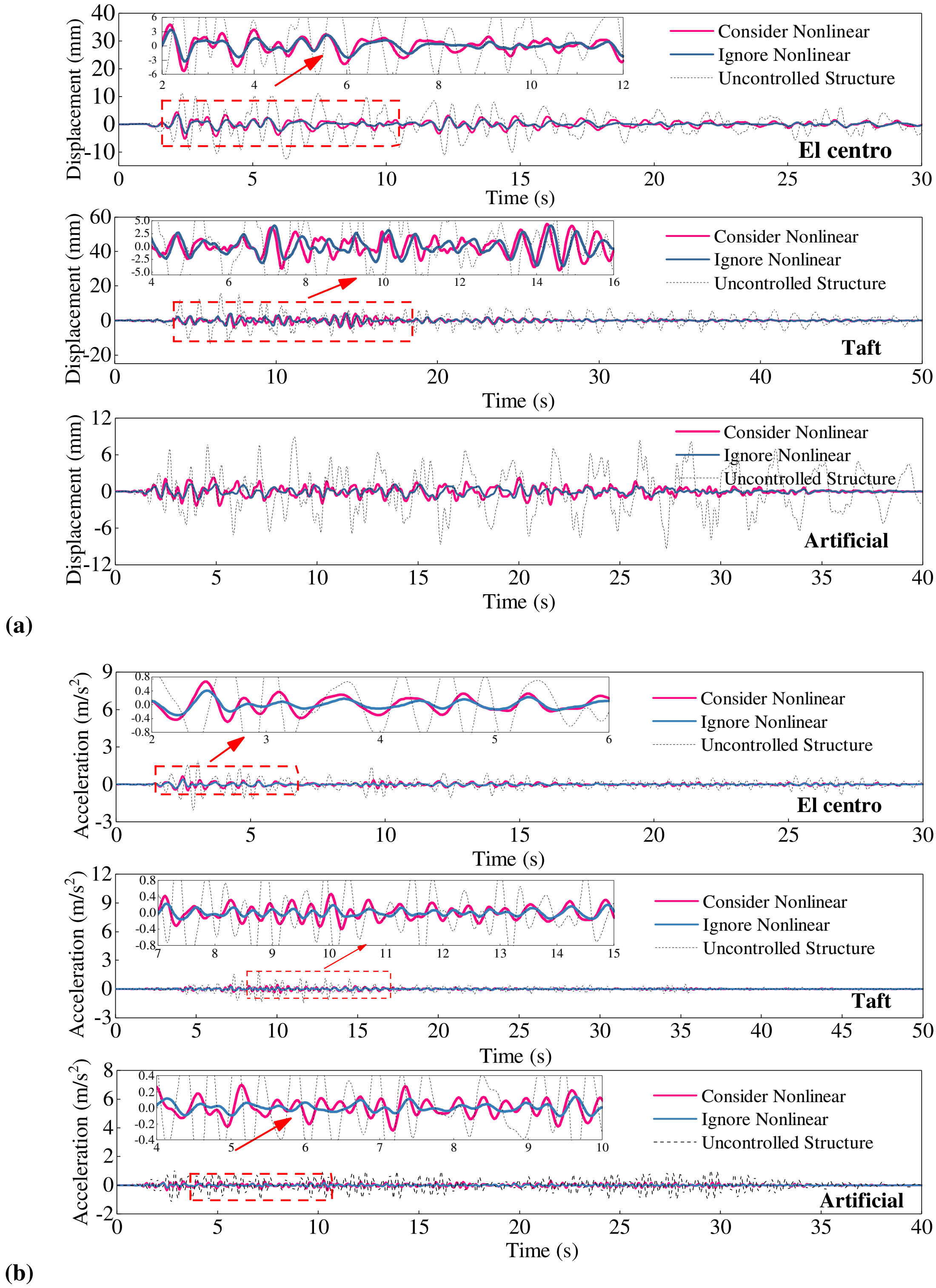

Fig. 11. Time histories of structural responses of the proportionally damped frame at roof. (a) roof displacement; (b) roof acceleration.

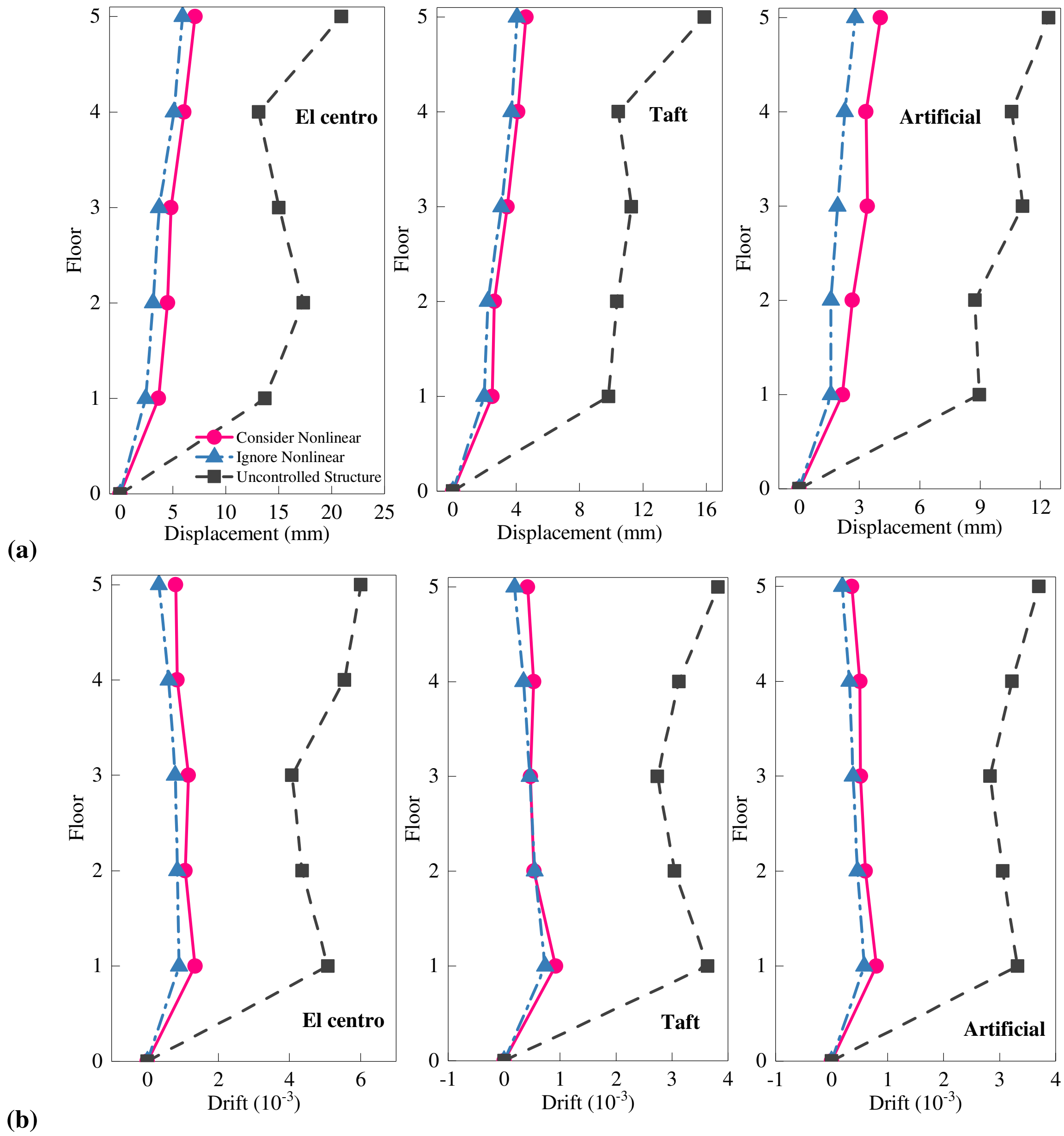

Fig. 12. Lateral structural response envelope of the proportionally damped frame. (a) Lateral displacement envelope; (b) Lateral drift envelope.

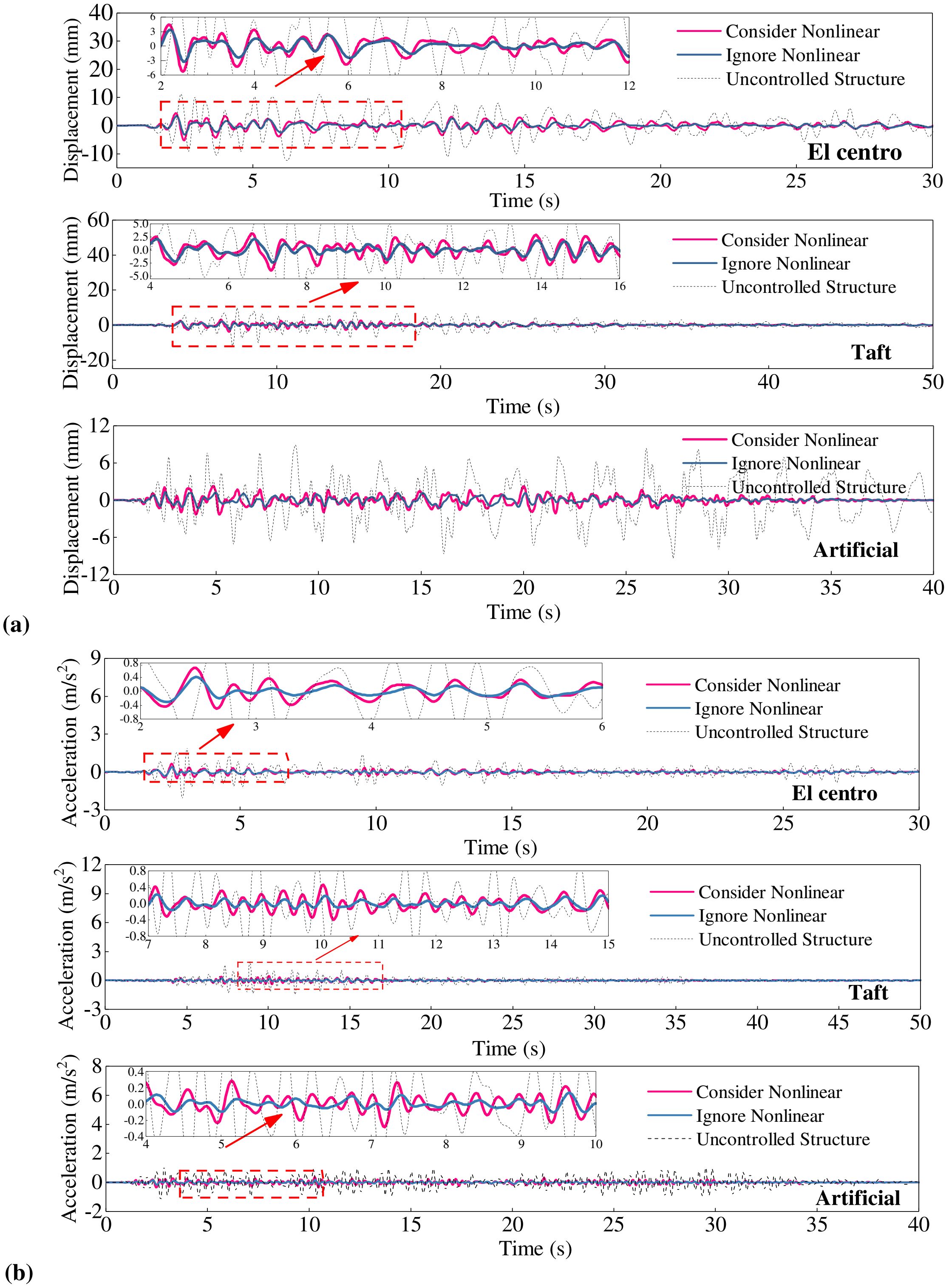

Fig. 13 Time histories of structural responses of the proportionally damped frame at roof. (a) roof displacement; (b) roof acceleration.

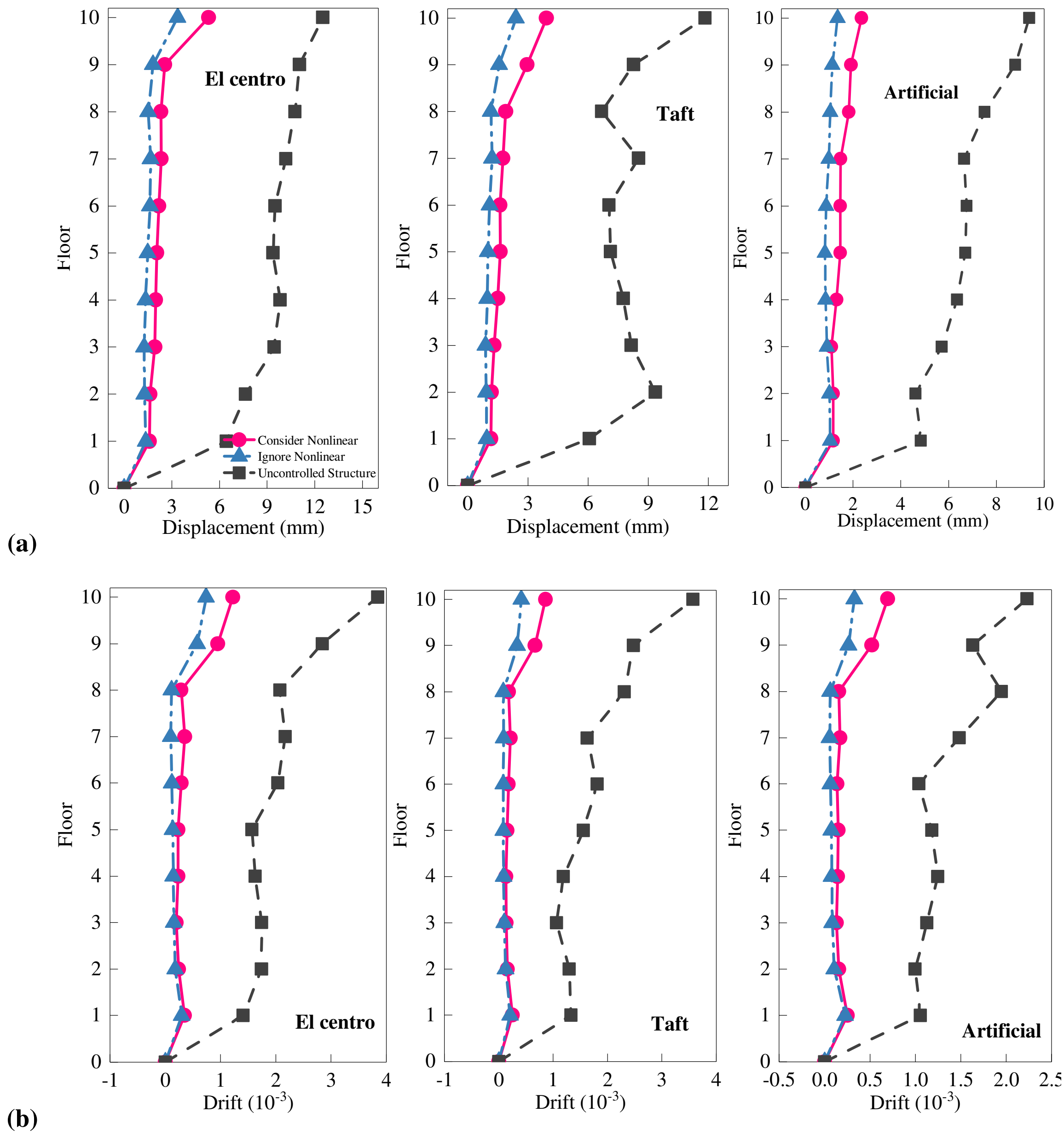

Fig. 14 Lateral structural response envelope of the non-proportionally damped frame. (a) Lateral displacement envelope; (b) Lateral drift envelope.

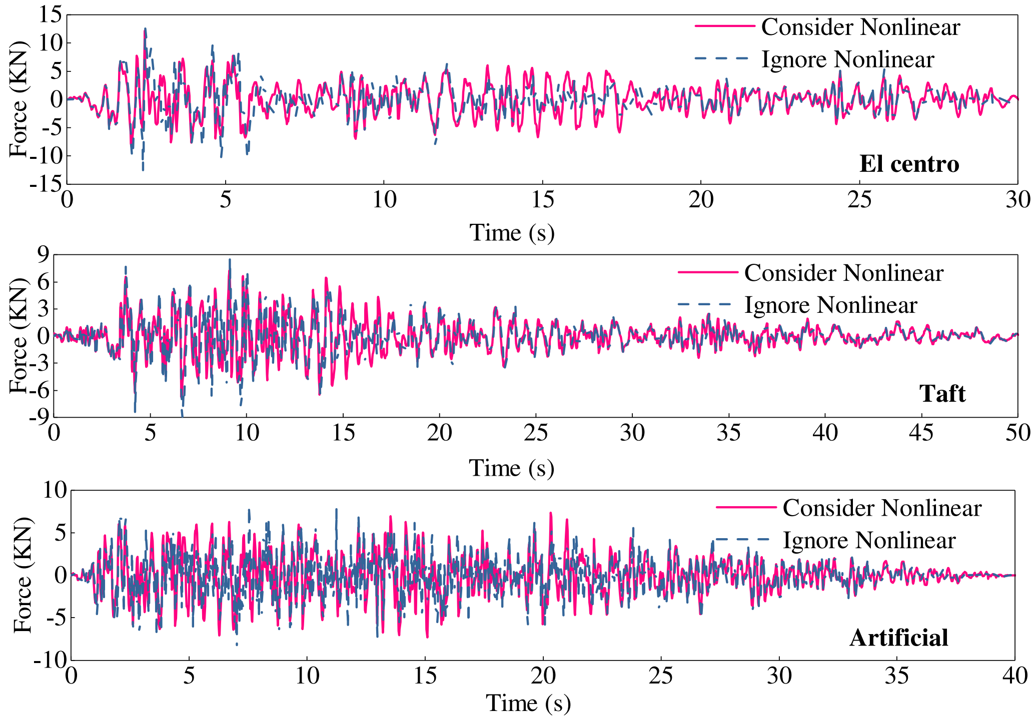

(a)

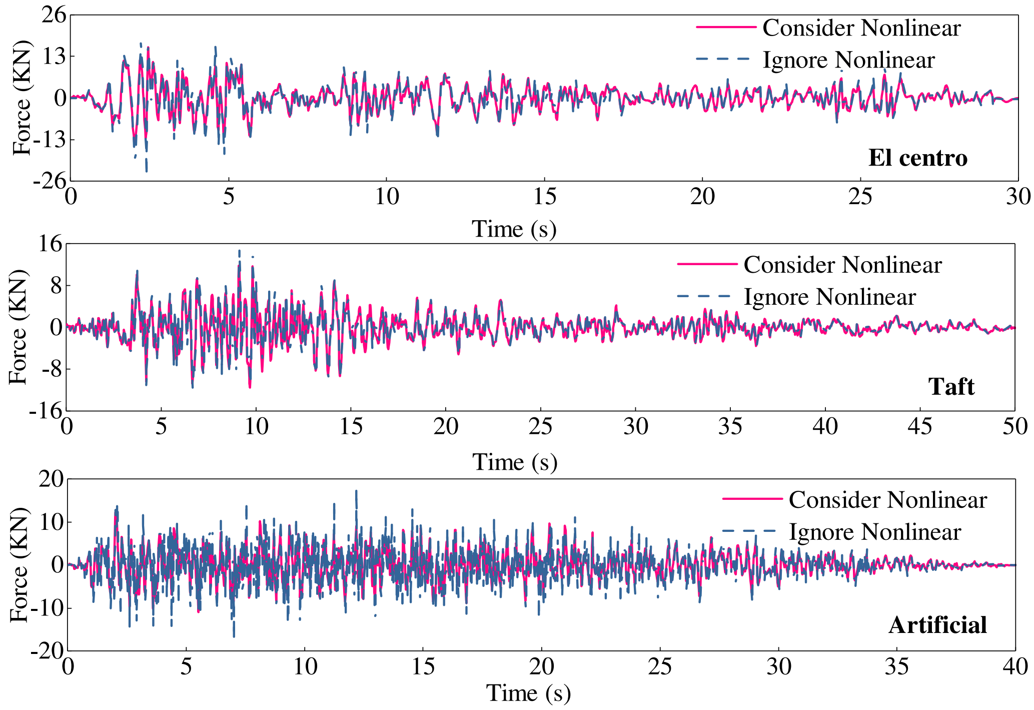

(b)

Fig. 15 Time histories of damping force of VE damper in 1floor. (a) the proportionally damped frame; (b) the non-proportionally damped frame.

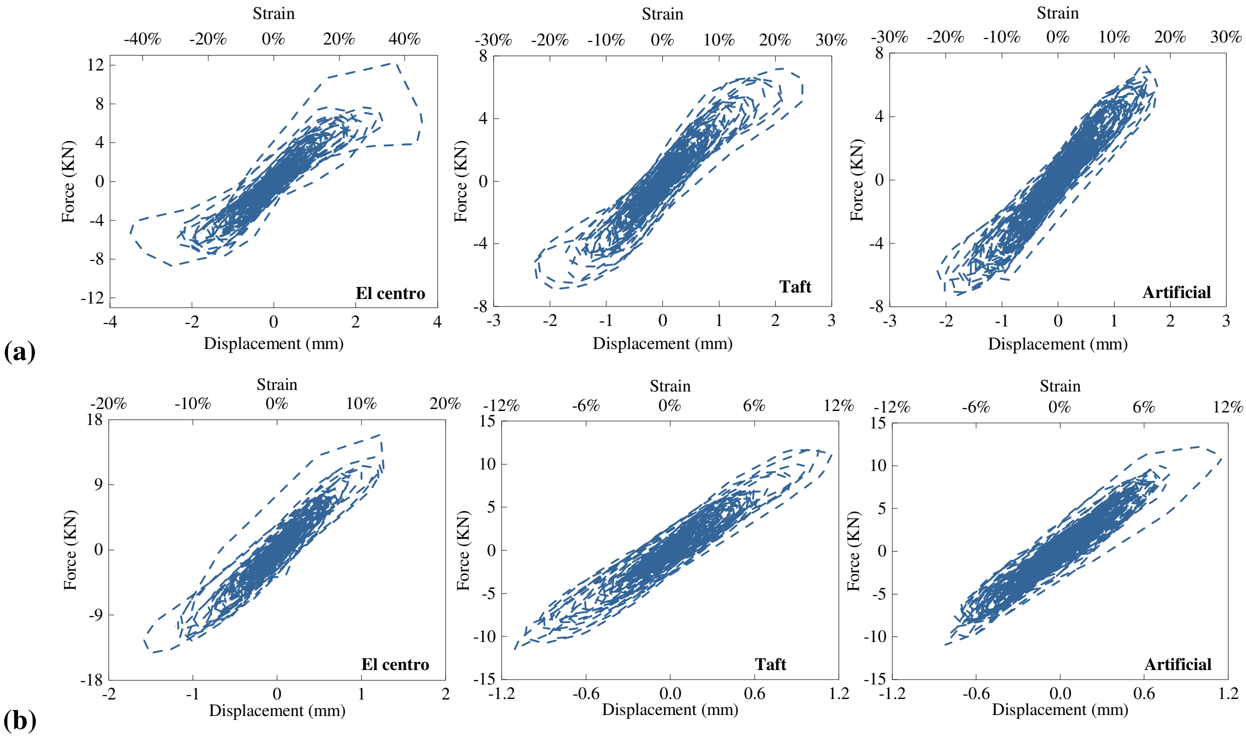

Fig. 16 Hysteresis curves VE damper in 1floor. (a) the proportionally damped frame; (b) the non-proportionally damped frame.

Tables

Table 1 Experiment protocol

Test group	γ	ω(Hz)	T(°C)
1	30%	0.5,1, 2, 4, 6, 8	15
	30%, 50%, 70%, 90%, 110%, 130%, 150%, 170%, 190%,	0.5	24
	40%	0.5	0, 10, 20, 30, 40, 50
2	15%	0.5,1, 2, 4, 6, 8	28
	20%, 40%, 60%, 80%, 100%, 120%, 140%, 160%, 180%,200%	0.5	24
	40%	1.0	0, 10, 20, 30, 40, 50

Table 2 Storage modulus and loss factor of the VE damper under different strains

Strain	Storage modulus G_1(KPa)	Loss factor η
30%	826	0.176
50%	745	0.169
100%	642	0.151
150%	593	0.124
180%	531	0.106
200%	230	0.087

Table 3 Parameters of three models

Model List	Model Parameters
Proposed model	$p_0 = 467.6, q_0 = 4.0, T_0 = 195.4, \kappa_1 = 0.175, \kappa_2 = -0.367, r = 0.307$
Model 1	$q_0 = 0.237, q_1 = 1910.538, T_0 = 1032.843, r = 0.142$
Model 2	$q_0 = 0.318, q_1 = 4.082, p_1 = 4.145, T_0 = 0.008, c = 1.417, d = 0.002$

Table 4a Calculation results of three models at different strains

Strain	Storage modulus G_1(KPa)				Loss factor η			
	Test data	Proposed model	Model 1	Model 2	Test data	Proposed model	Model 1	Model 2
20%	923	759	720	676	0.177	0.155	0.152	0.161
40%	826	730	720	676	0.176	0.152	0.152	0.161
60%	745	700	720	676	0.169	0.149	0.152	0.161
80%	686	671	720	676	0.163	0.146	0.152	0.161
100%	587	642	720	676	0.176	0.142	0.152	0.161
120%	628	613	720	676	0.142	0.138	0.152	0.161
140%	611	584	720	676	0.126	0.133	0.152	0.161
160%	593	555	720	676	0.124	0.128	0.152	0.161
180%	558	526	720	676	0.123	0.123	0.152	0.161
200%	452	496	720	676	0.109	0.116	0.152	0.161

Table 4b Calculation results of three models at different frequencies

Frequency ω(Hz)	Storage modulus G_1(KPa)				Loss factor η			
	Test data	Proposed model	Model 1	Model 2	Test data	Proposed model	Model 1	Model 2
0.5	735	736	703	631	0.134	0.141	0.150	0.161
1.0	774	783	751	787	0.139	0.164	0.155	0.161
2.0	828	841	804	894	0.172	0.189	0.160	0.161
4.0	877	913	863	947	0.195	0.215	0.164	0.160
6.0	888	963	900	963	0.207	0.231	0.167	0.160
8.0	917	1002	927	970	0.228	0.243	0.168	0.160

Table 4c Calculation results of three models at different temperatures

Temperature (°C)	Storage modulus G_1(KPa)				Loss factor η			
	Test data	Proposed model	Model 1	Model 2	Test data	Proposed model	Model 1	Model 2
0	1350	1175	888	948	0.346	0.293	0.166	0.160
10	965	959	837	913	0.289	0.241	0.162	0.161
20	832	821	788	854	0.191	0.194	0.158	0.161
30	709	730	742	768	0.139	0.153	0.154	0.161
40	623	669	697	663	0.121	0.119	0.149	0.161
50	588	628	655	560	0.120	0.093	0.144	0.161

Table 5 Maximum structural responses of the proportionally damped frame

	Roof displacement (mm)			Roof acceleration (m/s^2)			Drift (10^{-3})		
	El Centro	Taft	Artificial	El Centro	Taft	Artificial	El Centro	Taft	Artificial
Uncontrolled structure	20.92	15.86	12.41	4.87	3.11	3.02	6.01	3.82	3.70
Consider nonlinearity	7.09	4.61	4.04	2.32	1.30	1.34	1.35	0.92	0.79
Neglect nonlinearity	2.42	4.05	2.79	0.85	0.53	0.53	0.89	0.74	0.59

Table 6 Maximum structural responses of the non-proportionally damped frame

	Roof displacement (mm)			Roof acceleration (m/s^2)			Drift (10^{-3})		
	El Centro	Taft	Artificial	El Centro	Taft	Artificial	El Centro	Taft	Artificial
Uncontrolled structure	12.50	11.83	9.37	2.10	1.93	1.20	3.84	3.57	2.23
Consider nonlinearity	5.30	3.93	2.35	0.66	0.46	0.37	1.23	0.85	0.70
Neglect nonlinearity	3.36	2.41	1.36	0.40	0.23	0.18	0.74	0.41	0.32

Table 7 Max damping force of VE damper in 1floor.

Max damping force (KN)	The proportionally damped frame			The non-proportionally damped frame		
	El Centro	Taft	Artificial	El Centro	Taft	Artificial
Consider nonlinearity	12.26	7.27	7.32	15.90	11.75	12.24
Neglect nonlinearity	12.72	9.08	8.68	24.19	15.01	17.63

Figure list

Figure 14. Lateral structural response envelope of the non-proportionally damped frame. (a) Lateral displacement envelope; (b) Lateral drift envelope.

Figure 15. Time histories of damping force of VE damper in 1floor. (a) the proportionally damped frame; (b) the non-proportionally damped frame.

Figure 16. Hysteresis curves VE damper in 1floor. (a) the proportionally damped frame; (b) the non-proportionally damped frame.

Table list